

# Solution-Processed Low Threshold Vertical Cavity Surface Emitting Lasers from All-Inorganic Perovskite Nanocrystals

Wang, Yue; Li, Xiaoming; Nalla, Venkatram; Zeng, Haibo; Sun, Handong

2017

Wang, Y., Li, X., Nalla, V., Zeng, H., & Sun, H. (2017). Solution-Processed Low Threshold Vertical Cavity Surface Emitting Lasers from All-Inorganic Perovskite Nanocrystals. *Advanced Functional Materials*, 27(13), 1605088-.

<https://hdl.handle.net/10356/83307>

<https://doi.org/10.1002/adfm.201605088>

---

© 2017 WILEY-VCH Verlag GmbH & Co. KGaA, Weinheim. This is the author created version of a work that has been peer reviewed and accepted for publication by *Advanced Functional Materials*, WILEY-VCH Verlag GmbH & Co. KGaA, Weinheim. It incorporates referee's comments but changes resulting from the publishing process, such as copyediting, structural formatting, may not be reflected in this document. The published version is available at: [<http://dx.doi.org/10.1002/adfm.201605088>].

*Downloaded on 26 Aug 2022 19:30:35 SGT*

1     **Solution-processed low threshold vertical cavity surface emitting lasers**  
2                     **from all-inorganic perovskite nanocrystals**

3             Yue Wang<sup>1</sup>, Xiaoming Li<sup>2,3</sup>, Venkatram Nalla<sup>4</sup>, Haibo zeng<sup>2\*</sup>, Handong Sun<sup>1,4\*</sup>

4     <sup>1</sup>Division of Physics and Applied Physics, School of Physical and Mathematical Sciences,  
5     Nanyang Technological University, Singapore 637371, Singapore

6     <sup>2</sup>Institute of Optoelectronics & Nanomaterials, College of Materials Science and Engineering  
7     Nanjing University of Science and Technology Nanjing, 210094, China

8     <sup>3</sup>State Key Laboratory of Mechanics and Control of Mechanical Structures, College of Materials  
9     Science and Engineering, Nanjing University of Aeronautics and Astronautics, Nanjing 210085,  
10    China

11    <sup>4</sup>Centre for Disruptive Photonic Technologies (CDPT), Nanyang Technological University,  
12    Singapore 637371, Singapore

13    \* Authors to whom correspondence should be addressed, electronic email: [hdsun@ntu.edu.sg](mailto:hdsun@ntu.edu.sg),  
14    [zeng.haibo@njust.edu.cn](mailto:zeng.haibo@njust.edu.cn).

15    **Abstract:** Recently, all-inorganic cesium lead halide perovskite nanocrystals (IPNCs) (CsPbX<sub>3</sub>,  
16    X = Cl, Br, I) were discovered to possess superior optical gain properties appealing for solution-  
17    processed cost-effective lasers. Yet, the potential of such materials has not been exploited for  
18    practical laser devices, rendering the prospect as laser media elusive. Herein, we realized for the  
19    first time the challenging but practically desirable vertical cavity surface emitting lasers (VCSELs)  
20    based on the CsPbX<sub>3</sub> IPNCs, featuring low threshold (9 μJ/cm<sup>2</sup>), unidirectional output (beam  
21    divergence of ~3.6°) and favorable stability. The lasing wavelength can be tuned across red, green  
22    and blue region maintaining comparable thresholds, which is promising in developing single  
23    source-pumped full-color visible lasers. It is fully demonstrated that the characteristics of the

24 VCSELS can be versatily engineered by independent adjustment of the cavity and solution  
25 processable nanocrystals. Our results represent a significant leap towards practical laser sources  
26 leveraging on the advantageous CsPbX<sub>3</sub> IPNCs.

27

28

29

30

31

32

33

34

35

36

37

38

39

40

41

42

43 Solution-processed gain materials are being pursued with the promise to revolutionize the  
44 vacuum-based epitaxial semiconductor lasers aiming at developing low-cost yet high-  
45 performance laser source<sup>1</sup>. Colloidal quantum dot (CQD) has been recognized as the ideal  
46 candidate due to the tunable emission color, enhanced optical properties and facile solution  
47 processibility<sup>2-4</sup>. Ever since the first demonstration of stimulated emission from metal-  
48 chalcogenide CQDs in 2000<sup>2</sup>, significant progress has been made in improving the lasing  
49 performance<sup>5, 6</sup>. However, the relatively low absorption cross-section and the high optical loss  
50 due to carrier trapping and Auger recombination (AR) still hinder the advance of CQD-lasers,  
51 especially in the short visible spectral range of blue and green<sup>7, 8</sup>.

52 In the past years, the organic–inorganic halide perovskites, which have demonstrated  
53 impressive photovoltaic performance<sup>9, 10</sup>, were also discovered to be potential optical gain  
54 media<sup>11, 12</sup>. However, the commercial aspirations may be stifled by the inherent instability of  
55 these hybrid perovskites<sup>11, 12</sup>. More recently, the newly engineered all-inorganic cesium lead  
56 halide (CsPbX<sub>3</sub> (X=Cl, Br and I)) perovskite nanocrystals are resurging as a superior optical gain  
57 material because of the large optical absorption cross-section, large exciton binding energy, high  
58 photoluminescence (PL) quantum yield and relatively low AR loss<sup>13, 14</sup>. Importantly, these all-  
59 inorganic perovskite nanocrystals (IPNCs) show much enhanced endurance to ambient  
60 environment than the organic-inorganic analogues<sup>13, 15, 16</sup>. Compared to traditional metal-  
61 chalcogenide CQDs, these CsPbX<sub>3</sub> IPNCs feature in narrow emission spectra, simple fabrication  
62 process, ease of color tunability by anion exchange, superior optical gain properties and so on<sup>17-20</sup>.  
63 As a result, these new emerging CsPbX<sub>3</sub> IPNCs can be envisioned as the promising solution  
64 towards inexpensive laser sources in the future.

65 So far, lasers based on single CsPbX<sub>3</sub> nanowire have been reported<sup>21, 22</sup>. Regarding lasers  
66 made from the ensemble of inorganic perovskite nanocrystals, only whispering gallery mode and  
67 random lasers which are among the easiest configurations for lasers have been demonstrated as a  
68 proof of concept<sup>13, 14</sup>. However, both of these laser types lack directionality, one of the most  
69 important advantages of a laser. Moreover, all of the above lasing demonstrations fall in multi-  
70 mode operation<sup>13, 14</sup>. In laser physics and applications, obtaining single-mode lasing is crucial  
71 since multi-mode operation will deteriorate the color purity and temporal stability by mode  
72 oscillation<sup>23, 24</sup>. Due to the typical large cavity length to provide sufficient gain for lasing action  
73 and the relatively broad gain bandwidth of traditional lasing materials, achieving single-mode  
74 lasing is still challenging<sup>23, 24</sup> and remains unaccomplished for CsPbX<sub>3</sub> IPNCs.

75 Vertical cavity surface emitting laser (VCSEL) is an important and much desired laser type  
76 which finds a broad range of applications like optical communication, high density optical storage,  
77 laser display, parallel optical computing and signal processing because of its ability to form 2-  
78 dimensional arrays, surface normal emission characteristics and high beam quality output  
79 ensuring easy coupling into an optical fibre<sup>25,26</sup>. For any given gain materials, VCSELs represent  
80 the most tough laser configuration determined by the stringent criteria between gain and loss<sup>6,25</sup>.  
81 As such, most surface normal devices were previously developed from complicated epitaxial  
82 growth of semiconductor heterostructures of many layers in which both bandgap alignment and  
83 lattice mismatch are big concerns<sup>27-30</sup>. The unavailability of independently adjusting the cavity  
84 and the active gain materials in an epitaxy based VCSEL makes material selection a constraint  
85 and the device cost ineffective. Thus, alternative fabrication of VCSELs with simplified  
86 processing is very appealing. Herein, we realized for the first time the high-performance VCSELs  
87 from solution-processed CsPbX<sub>3</sub> IPNCs. A clear evolution from spontaneous emission to lasing  
88 in the device upon optical pumping was manifested by the spectral narrowing, nonlinear increase  
89 of the PL intensity, drastic reduction of PL lifetime and remarkable decrease of output beam  
90 divergence. Both multi-mode and single-mode lasing operation have been achieved by tuning the  
91 cavity length. Thanks to the superior optical gain properties of the CsPbBr<sub>3</sub> IPNCs and the good  
92 match between the gain profile and the high reflectivity band of the distributed Bragg reflectors  
93 (DBRs), the lasing threshold of the IPNC-VCSELs is so low that quasi-continuous wave (q-CW)  
94 pumping is feasible. In contrast to traditional metal-chalcogenide CQD based lasers, where the  
95 thresholds for the green and blue are typically much higher than that of the red<sup>6</sup>, these CsPbX<sub>3</sub>  
96 IPNC-VCSELs lase with comparable thresholds across the whole visible spectral range, which is  
97 promising in achieving single source-pumped full-color lasers. Our results highlight the resurging  
98 CsPbX<sub>3</sub> IPNCs in developing the challenging but practical lasers and shed light on the feasibility  
99 of independent adjustment of cavity and gain materials for the IPNC-VCSELs, which represent a  
100 great progress towards advanced laser sources based on the advantageous CsPbX<sub>3</sub> IPNCs.

## 101 **Results**

102 **Modification of spontaneous emission from CsPbBr<sub>3</sub> IPNCs by microcavity effect.** The  
103 CsPbX<sub>3</sub> IPNCs adopted here were synthesized following the method reported by Protesescu et  
104 al.<sup>17</sup> with slight adjustment<sup>13</sup>. The absorption and emission spectra of the CsPbBr<sub>3</sub> IPNCs are  
105 shown in Supplementary Fig. 1b, revealing the emission peak of ~504 nm with a narrow full-  
106 width at half maximum (FWHM) of ~21 nm. The corresponding transmission electron  
107 microscope (TEM) image (Supplementary Fig. 1a) displays the cubic shape with an edge length

108 of ~9 nm. To build the vertical microcavity, the commercially available dielectric DBRs  
109 consisted of 25 pairs of SiO<sub>2</sub>/TiO<sub>2</sub> quarter-wave layers were employed as the high-reflective  
110 mirrors. Figure 1a displays the reflection spectrum of a DBR used here, which exhibits a stop-  
111 band from 430 nm to 570 nm, matching the PL spectrum of CsPbBr<sub>3</sub> IPNCs (see broadband  
112 reflection spectrum in Supplementary Fig. 2). The reflectivity was determined to be as high as  
113 99.6% at ~500 nm. To sandwich the CsPbBr<sub>3</sub> IPNCs between two DBRs so as to form the  
114 prototypical VCSEL, the highly concentrated CsPbBr<sub>3</sub> IPNCs solution was spin-coated onto the  
115 top surface of a DBR, then, another DBR was brought upside-down in contact to the CsPbBr<sub>3</sub>  
116 IPNC film and finally fixed with glue. The schematic diagram (Fig. 1b), photograph  
117 (Supplementary Fig. 3) and the corresponding reflection spectrum ((Supplementary Fig. 2) of the  
118 final device are presented. Prior to the lasing investigation, the modification of spontaneous  
119 emission from CsPbX<sub>3</sub> IPNCs by the optical microcavity was interrogated, which could reflect  
120 the quality of the complete DBR resonator. Figure 1a shows the typical PL spectrum from the  
121 CsPbBr<sub>3</sub> IPNCs inserted within the cavity collected at 0° with respect to the surface normal (see  
122 Methods for details). In contrast to the PL spectrum from CsPbX<sub>3</sub> IPNCs spin-coated on a single  
123 DBR substrate, the PL within the cavity manifests multiple interference peaks, visualizing the  
124 presence of Fabry-Perot cavity effect. It is worth to note that the spiked emission is not laser but  
125 spontaneous emission modified by interference effect, which is further demonstrated by the  
126 following lifetime measurements (Fig. 2c). The resonant peaks can be assigned to mode numbers  
127 indexed as 29-33 based on the equation<sup>31</sup>:  $m\lambda = 2nL$ , where  $m$  is the mode number,  $\lambda$  is the  
128 emission wavelength,  $n$  is the refractive index of the CsPbX<sub>3</sub> IPNC film,  $L$  is the effective cavity  
129 length.  $L$  is estimated to be 4 μm assuming  $n=2^{13}$ . By changing the thickness of the CsPbBr<sub>3</sub>  
130 IPNC film, the optical modes of the cavity and thus the PL spectrum can be tuned as exemplified  
131 in Supplementary Fig. 4. The slight red-shift of the envelop of the emission comb relative to the  
132 free-space emission spectrum can be attributed to the reabsorption effect due to the multipass of  
133 the radiation inside the cavity<sup>24</sup>. Furthermore, the spatial distribution of the radiation and the  
134 angle ( $\theta$ ) dependent PL spectrum from the device were examined by angle-resolved PL  
135 measurement (see Methods for details). It is found that the optical mode wavelengths gradually  
136 shift to blue as the detection angle increases (Fig. 2a), which quantitatively follows the equation:  
137  $m\lambda = 2nL\sqrt{n^2 - \sin^2\theta}$  (Supplementary Fig. 5). Such behavior states nothing but that the  
138 radiation propagation angle inside the cavity and the detection angle are correlated by Snell's law  
139 (see detailed deviations in Supporting Information)<sup>1,31</sup>, further confirming that the discrete peaks  
140 originate from the Fabry-Perot interference. Notably, the radiation from the microcavity is much  
141 narrowed in space with respect to that from free-space CsPbBr<sub>3</sub> IPNCs (Fig. 2b), indicating that

142 spatially confined emission is obtained by the microcavity effect, which may shed light on  
143 developing CsPbX<sub>3</sub> IPNC-based light emitting diodes with directional radiation. Finally, the  
144 carrier dynamics of CsPbBr<sub>3</sub> IPNCs within/without microcavity was inspected by a streak camera  
145 system (Fig. 2c) (see the corresponding spectrograms in Supplementary Fig. 6). It is found that  
146 the PL decay curve within microcavity is almost identical to that in free space. A reduction of PL  
147 lifetime due to Purcell effect is not observed which can be attributed to the long cavity length and  
148 that the cavity mode only confined in one dimension<sup>32</sup>.

149 **Vertical cavity surface emitting lasers from CsPbBr<sub>3</sub> IPNCs.** The stimulated emission from  
150 the close-packed thin film of the CsPbBr<sub>3</sub> IPNCs was first studied by stripe pumping  
151 configuration<sup>13, 33</sup> to exam the optical gain. As increasing the pumping density, the development  
152 of stimulated emission revealed by a much narrowed emission peak (FWHM: ~6.5 nm) can  
153 readily occur from our sample with a threshold of ~18 μJ/cm<sup>2</sup> (Supplementary Fig. 7). Such a  
154 low-threshold optical gain from CsPbBr<sub>3</sub> IPNCs in combination with the favorable coupling  
155 between the emission and the cavity modes motivates us to pursue CsPbBr<sub>3</sub> IPNC-based VCESLs.  
156 In doing so, the pump laser beam (400 nm, 100 fs) was focused by a circular lens (focus length: 5  
157 cm) onto the device vertically, and the PL signal was collected from the surface normal of the  
158 cavity. A 30% reflection by the DBR for pump wavelength was extracted and counted in  
159 determining the final pump intensity. Figure 3a displays the evolution of PL spectra from the  
160 device as a function of pump intensity. Under relatively low pump intensities (< 11 μJ/cm<sup>2</sup>), the  
161 PL spectra are dictated by spontaneous emission shaped by the cavity mode. With the increase of  
162 pump intensity, one of the discrete peaks with wavelength close to the stimulated emission  
163 spectra grows much faster than the others, which is accompanied by dramatic narrowing of the  
164 line-width down to ~0.6 nm. Figures 3b and c depict the change of PL intensity and the FWHM  
165 of the peaks corresponding to mode numbers from 29 to 33, respectively. The abrupt increase of  
166 the PL intensity and sudden decrease of the line-width of a particular peak indicate the  
167 achievement of lasing action<sup>1, 34, 35</sup>. The lasing threshold ( $P_{th}$ ) is derived to be as low as 11 μJ/cm<sup>2</sup>,  
168 which is much lower than that of the CdSe/CdZnS CQDs (65 μJ/cm<sup>2</sup>), under similar conditions<sup>6</sup>.  
169 Importantly, due to the much larger free spectral range ( $FSR$ ) of ~16 nm determined by the short  
170 cavity length than the stimulated emission line-width (6.5 nm), single-mode lasing operation was  
171 achieved. It should be noted that although the lasing peak locates at the blue side of the emission  
172 comb, it is actually on the red side of the spontaneous emission maximum of CsPbBr<sub>3</sub> IPNCs  
173 (Supplementary Fig. 8), in agreement with that the optical transition of the laser originates from  
174 the biexciton recombination<sup>13, 36, 37</sup>.

175 To further verify the development of lasing, the PL dynamics as a function of pump intensity  
176 was investigated. Under pump intensity ( $0.1 P_{th}$ ) of much lower than the threshold, the PL decay  
177 resembles the spontaneous emission trace. With the increase of pump intensity ( $0.8 P_{th}$ )  
178 approaching the threshold, a much faster decay channel, corresponding to the Auger  
179 recombination, appears. As the pump intensity ( $1.3 P_{th}$ ) surpasses the threshold, the PL decay  
180 suddenly collapses to  $<50$  ps, limited by the temporal resolution of the streak camera system,  
181 indicating the onset of lasing action<sup>38</sup>.

182 Coherence and directionality are two basic features of a laser but are rarely examined in  
183 CQDs based lasers. Herein the directionality of the output radiation above and below the  
184 threshold is assessed by a CCD camera located 15 mm away from the laser device (inset in Fig.  
185 3a) as well as angle-resolved PL measurement (Supplementary Fig. 9). We can see that when the  
186 pump intensity ( $1.3 P_{th}$ ) exceeds the threshold, the divergence of the output signal remarkably  
187 decreases from  $15^\circ$  for spontaneous emission below  $P_{th}$  to  $3.6^\circ$ , thus a directional emission was  
188 obtained in our IPNC-VCSEL. Moreover, a clear interference pattern (Supplementary Fig. 10a)  
189 can be observed by using the conventional Michelson interference experiment<sup>39,40</sup>. From the plot  
190 of the visibility ( $V = \frac{I_{max}-I_{min}}{I_{max}+I_{min}}$ , where  $I_{max}$  and  $I_{min}$  represent the intensities at the fringe maxima  
191 and minimum) as a function of detuning time or optical path difference<sup>39,40</sup>, the coherence time ( $\tau$ )  
192 of  $\sim 1$  ps can be derived (Supplementary Fig. 10c).

193 Finally, we test the stability of the device by monitoring the lasing peak intensity versus time  
194 at pump intensity of  $1.5 P_{th}$  (pulse-width: 100 fs; repetition rate: 1KHz) (Supplementary Fig. 11).  
195 Thanks to the robustness of the CsPbBr<sub>3</sub> IPNCs, the output signal can maintain 80% of its initial  
196 value for more than one hour, which far excels the CdSe/CdZnS CQD-lasers<sup>6</sup>.

197 Inspired by the excellent laser performance under femtosecond laser pump, it is highly  
198 promising to explore our IPNC-VCSEL pumped in the q-CW regime by a compact nanosecond  
199 laser<sup>7,41</sup>, which would be more practical and cost-effective. A ns laser pump is called the q-CW  
200 just because the pump duration is much longer than that of the effective gain ( $\sim 35$  ps)<sup>42</sup>. Figure 4a  
201 shows the pump intensity dependent PL spectra pumped by a Q-switched nanosecond laser  
202 (pulse-width: 5 ns; repetition rate: 20 Hz; wavelength: 400 nm). The onset of lasing action is  
203 unambiguously evidenced by the spectral narrowing and nonlinear increase of the PL intensity  
204 with respect to the pump intensity (inset in Fig. 4a) with a low threshold of  $900 \mu\text{J}/\text{cm}^2$ . To the  
205 best of our knowledge, this is the first demonstration of CQD-VCSEL operating in q-CW regime,  
206 which represents a significant step towards continuous wave and electrical pumping. The lasing



207 stability under nanosecond pumping is also examined (Supplementary Fig. 11). It is found that  
208 the lasing can last over one hour with losing only 50% of initial peak intensity. The faster  
209 decrease of the lasing intensity compared to that under femtosecond pump suggests the more  
210 serious thermal issue for long pump pulse duration<sup>36</sup>. So the effective thermal management (heat  
211 roll-off) shall be one of the major issues to address for future work toward stable CW operation<sup>36</sup>,  
212 <sup>43</sup>.

213 Furthermore, we demonstrate that multi-mode lasing operation can be produced in our  
214 IPNC-VCSELS via tuning the *FSR* to be smaller than the stimulated emission bandwidth which is  
215 enabled by increasing the effective cavity length (*L*) or film thickness of CsPbBr<sub>3</sub> IPNCs. Figure  
216 4b illustrates the typical double mode lasing from the IPNC-VCSEL with *FSR* of ~6.2 nm and *L*  
217 of ~10.3 μm. Due to the longer cavity path and thus the larger round-trip gain, the lasing threshold  
218 further reduces to ~9.0 μJ/cm<sup>2</sup> (inset in Fig. 4b).

219 **Full-color VCSELS from CsPbX<sub>3</sub> IPNCs with comparable thresholds.** For traditional metal-  
220 chalcogenide CQDs, the lasing wavelength is generally tuned by changing the dot size because of  
221 the band gap limit<sup>2,6</sup>. For example, smaller dot size is necessitated to obtain green and blue lasers  
222 than that for red ones<sup>6</sup>. However, the optical loss including nonradiative AR and carrier trapping  
223 becomes more serious and the absorption cross-section reduces as the dot decreases, making the  
224 CQDs lase in short visible region challenging<sup>2,8</sup>. Despite that lasing has been demonstrated from  
225 CQDs across the full visible range<sup>6</sup>, the pump thresholds differ dramatically for red, green and  
226 blue colors, which hinders the realization of integrated full-color lasers with single pumping  
227 source<sup>44</sup>. In contrast, the emission color of CsPbX<sub>3</sub> IPNCs can be facily tailored by composition  
228 control<sup>17, 18</sup>. By inserting the blue-emitting CsPb(Br/Cl)<sub>3</sub> IPNCs and red-emitting CsPb(I/Br)<sub>3</sub>  
229 IPNCs into the DBR resonators (for the red-emitting CsPb(I/Br)<sub>3</sub> IPNC-VCSEL, the DBR with  
230 stop-band centered at 590 nm was employed (Supplementary Fig. 12)), we successfully achieved  
231 IPNC-VCSELS across the full visible region (Fig. 5) (see full-range spectra in Supplementary Fig.  
232 13 and Supplementary Fig. 14 for blue and red VCSELS, respectively). Notably, the lasing  
233 thresholds for the red (19.0 μJ/cm<sup>2</sup>) and blue (25.5 μJ/cm<sup>2</sup>) are comparable to that of the green,  
234 which indicates our CsPbX<sub>3</sub> IPNC-VCSELS may hold great promise for developing the single  
235 source-pumped full-color visible and white lasers.

## 236 Discussion

237 We for the first time realized the tough yet practically desirable VCSELS based on the emerging  
238 solution-processable CsPbX<sub>3</sub> IPNCs. The CsPbX<sub>3</sub> IPNC-VCSELS operate at a very low threshold,

239 so that the q-CW pumping is made feasible. Such a low lasing threshold can be mainly attributed  
240 to the large absorption cross-section of the CsPbX<sub>3</sub> IPNCs, high PL quantum yield, relatively low  
241 Auger loss and the good match between the gain profile and the stop-band of the DBRs<sup>13, 14</sup>.  
242 Especially, the absorption cross-section of the CsPbX<sub>3</sub> IPNCs was disclosed to be orders of  
243 magnitude higher than those of the metal-chalcogenide CQDs<sup>13, 14, 42</sup>, which allows for the  
244 generation of excitons with denser concentration under the same pump density. Therefore, even  
245 though the CsPbX<sub>3</sub> IPNC-VCSELs stem from the biexciton recombination<sup>13, 37</sup>, the pump  
246 thresholds for lasing still remain several times lower than that of the CdSe/CdZnS CQDs under  
247 similar conditions which was claimed to lase in single exciton regime<sup>6</sup>. Another advantage of the  
248 CsPbBr<sub>3</sub> IPNCs may be its cubic crystal shape. In general, dense packing of the nanocrystals in  
249 the ensemble film is essential for high effective gain and thus a low lasing threshold. In this  
250 regard, the cubic shape of CsPbBr<sub>3</sub> IPNCs is advantageous over the spherical ones of II-VI group  
251 metal-chalcogenide CQDs. The directionality and coherence from the laser device was clearly  
252 revealed. Taking advantage of the short cavity length and the narrow gain spectrum (~6.5 nm),  
253 single-mode lasing was achieved, attractive for various application fields. Noticeably, it is facile  
254 to independently choose the cavity characteristics and CsPbX<sub>3</sub> IPNCs for optimal match so that  
255 red, green and blue VCSELs can be realized with comparable pump thresholds, which is  
256 extremely difficult for epitaxial semiconductors and traditional metal-chalcogenide CQDs. We  
257 envisage that further optimization of the CsPbX<sub>3</sub> IPNCs, such as engineering the core/alloyed-  
258 shell heterostructure to mitigate the Auger and trapping loss<sup>45</sup>, as well as adoption of proper  
259 thermal management in the device<sup>36</sup> could further reduce the lasing threshold and may eventually  
260 enable the continuous wave operation in the future.

## 261 **Methods**

262 **Synthesis of CsPbX<sub>3</sub> IPNCs.** Cs<sub>2</sub>CO<sub>3</sub> (0.8 g), OA (oleic acid, 2.5 mL) and of ODE (octadecene,  
263 30 mL) were mixed and kept in an argon atmosphere. The mixture was heated up to 130 °C for  
264 one hour. After that, the mixture was further heated up to 150 °C for reaction and lasted for 0.5  
265 hour. Then, the solution was cooled down to room temperature. On the other side, 10 mL ODE, 1  
266 mL OA and 0.36 mmol of PbX<sub>2</sub> (X=Cl, Br and I) were put together and kept in an argon  
267 atmosphere for one hour at temperature of 130 °C. Then, the solution was further heated up to  
268 160 °C for reaction for 10 minutes. Finally, the Cs-precursor (1 mL) was quickly added into the

269 solution and cooled down by ice. More information about the synthesis of CsPbX<sub>3</sub> IPNCs can be  
270 found in reference 13.

271 **Optical characterization.** To investigate the modification of spontaneous emission from CsPbX<sub>3</sub>  
272 IPNCs by microcavity effect, the same femtosecond laser source (excitation wavelength: 400 nm,  
273 pulse-width: 100 fs, repetition rate: 1000 Hz) was employed as that used in the following lasing  
274 studies to maintain consistency. The excitation intensity was kept very low (0.5 μJ/cm<sup>2</sup>), far less  
275 than the threshold. We also have tried the continuous wave He-Cd laser as the excitation source,  
276 where similar spiked emission was observed, further confirming the spiked emission is not laser.  
277 The angle dependent PL signal was recorded as a function of detection direction by a home-built  
278 fiber-optics system. In particular, the collection fiber with diameter of 200 μm was attached to a  
279 50 mm diameter rotating stage with the sample mounted at its center. The distance between the  
280 fiber and the sample is set as 15 mm. The other side of the fiber was coupled to a 320 mm  
281 monochromator combined with a charge coupled device detector. For the lasing investigation, the  
282 laser beam with wavelength of 400 nm generated by second harmonic generation from the seed  
283 with wavelength of 800 nm was focused by a circular lens (focus length: 5 cm) onto the VCSEL  
284 vertically, and the spot diameter on the sample was ~90 μm. The output signal was collected from  
285 the other side of the VCSEL by the above-mentioned fiber-optics system.

286

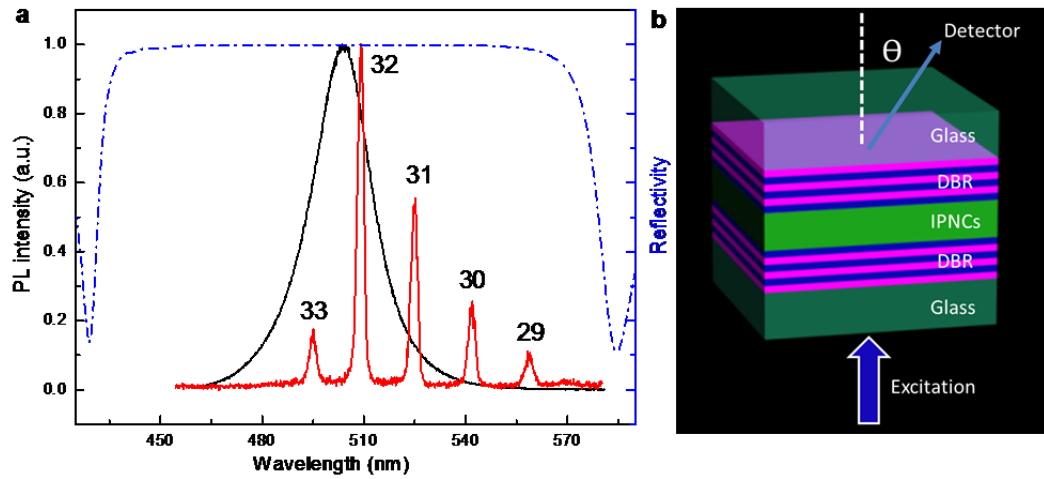
287

288

289

290

291



292 **Figure 1 | Modification of spontaneous emission from CsPbBr<sub>3</sub> IPNCs by presence of**  
 293 **microcavity.** (a) PL spectra from CsPbBr<sub>3</sub> IPNCs within (red line)/without (black line)  
 294 microcavity under low excitation intensity of 0.5 μJ/cm<sup>2</sup>. The blue dashed line represents the  
 295 reflectivity of the adopted DBR. (b) Schematic configuration of the CsPbBr<sub>3</sub> IPNC-VCSEL.

296

297

298

299

300

301

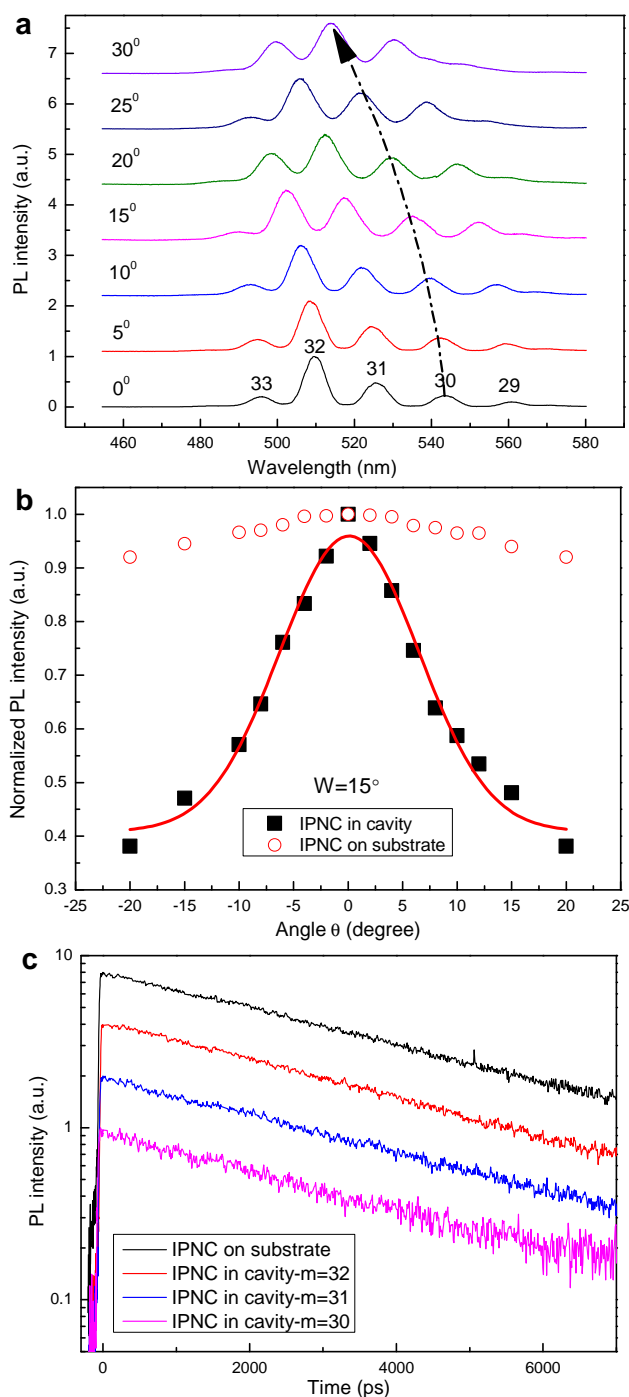
302

303

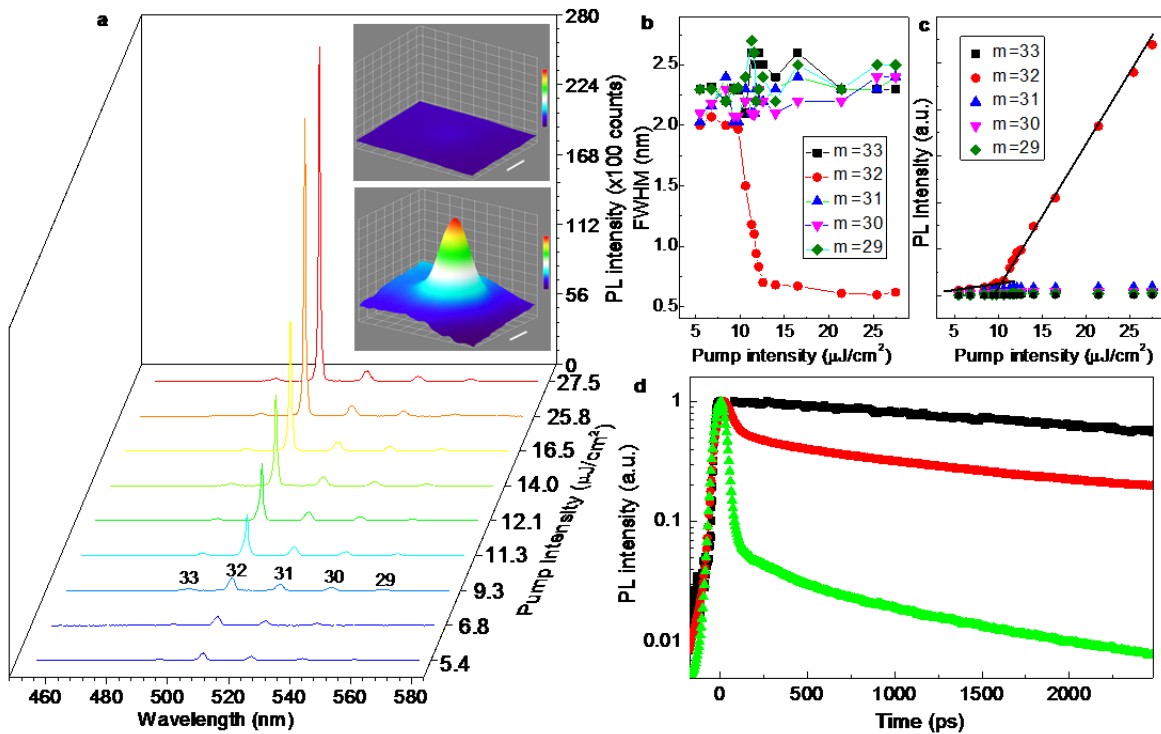
304

305

306



307 **Figure 2| Angle-resolved PL from CsPbBr<sub>3</sub> IPNCs within microcavity and PL dynamics. (a)**  
 308 **Detection angle dependent PL spectra from the CsPbBr<sub>3</sub> IPNCs within microcavity. (b)** Spatial  
 309 **distribution of the irradiation from CsPbBr<sub>3</sub> IPNCs within/without microcavity. The PL signal**  
 310 **greatly narrows with the presence of microcavity. The divergence is estimated to be 15° by**  
 311 **Gaussian fitting (red line). (c)** PL decay curves of CsPbBr<sub>3</sub> IPNCs within microcavity (mode  
 312 **number from 30 to 32) and that without microcavity.**



313 **Figure 3| Vertical cavity surface emitting lasers from CsPbBr<sub>3</sub> IPNCs. (a)** Pump intensity  
 314 dependent PL spectra from the device. Inset shows the output beam profiles below (5.4 μJ/cm<sup>2</sup>)  
 315 (upper one) and above (25.8 μJ/cm<sup>2</sup>) (bottom one) threshold. Scale bar is 1 mm. **(b)** Pump  
 316 intensity dependent FWHM of the modes indexed from 29 to 33. **(c)** Pump intensity dependent  
 317 PL intensity of the modes indexed from 29 to 33. **(d)** Pump intensity dependent PL decay curves  
 318 of the device (0.1 P<sub>th</sub> for the black curve, 0.8 P<sub>th</sub> for the red curve and 1.3 P<sub>th</sub> for the green curve)

319

320

321

322

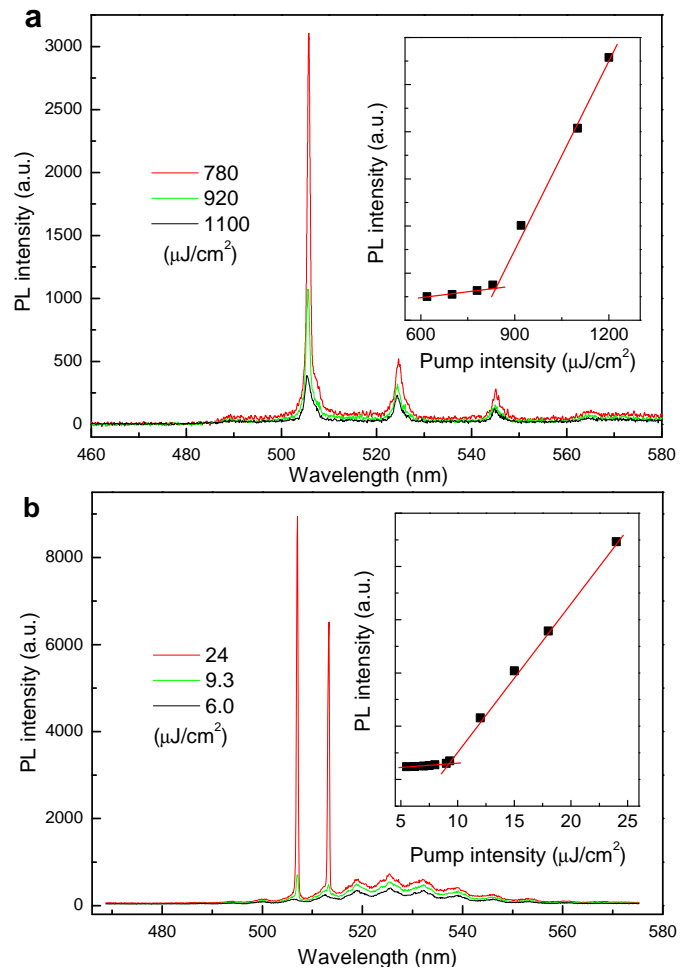
323

324

325

326

327



328 **Figure 4| Lasing operation in quasi-continuous wave regime and multi-mode lasing. (a)**  
 329 Nanosecond laser pumped PL spectra as a function of pump intensity. The inset shows the  
 330 integrated PL intensity over the sharp peak versus pump intensity. **(b)** Multi-mode lasing from the  
 331 CsPbBr<sub>3</sub> IPNC-VCSEL. The inset shows the integrated PL intensity over the sharp peaks versus  
 332 pump intensity.

333

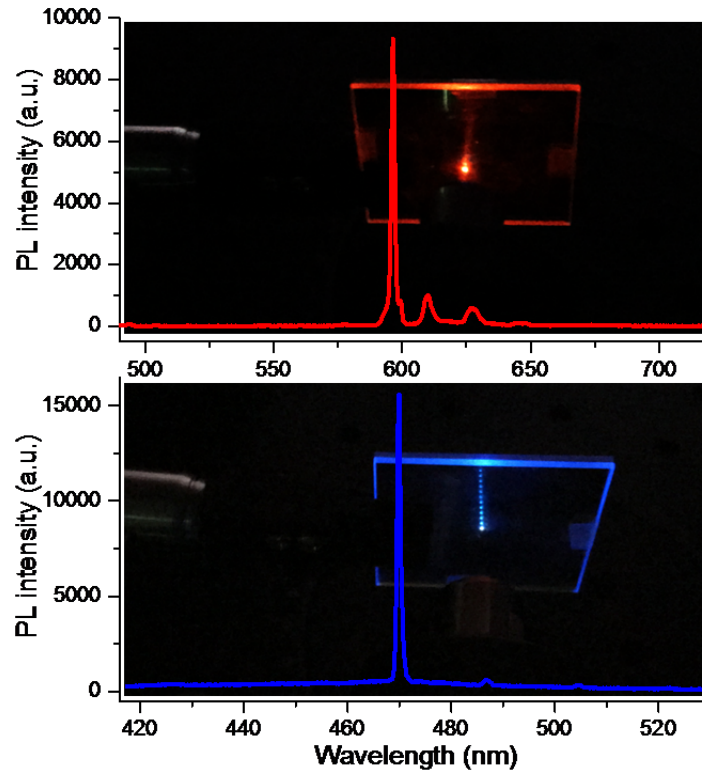
334

335

336

337

338



339 **Figure 5| Red and blue vertical cavity surface emitting lasers from CsPbX<sub>3</sub> IPNCs.** Red and  
 340 blue lasing spectra of vertical cavity surface emitting lasers from CsPb(I/Br)<sub>3</sub> and CsPb(Br/Cl)<sub>3</sub>  
 341 IPNCs under pump intensity of 30.5 and 38.2  $\mu\text{J}/\text{cm}^2$ , respectively. The corresponding  
 342 photograph of the device in operation is attached inside the plot.

343

344

345

346

347

348

349

350

351



- 352 1. Tessler, N., Denton, G.J. & Friend, R.H. Lasing from conjugated-polymer microcavities.  
353 *Nature* **382**, 695-697 (1996).
- 354 2. Klimov, V.I. et al. Optical gain and stimulated emission in nanocrystal quantum dots.  
355 *Science* **290**, 314-317 (2000).
- 356 3. Wang, Y. et al. Stimulated Emission and Lasing from CdSe/CdS/ZnS Core-Multi-Shell  
357 Quantum Dots by Simultaneous Three-Photon Absorption. *Adv. Mater.* **26**, 2954-2961  
358 (2014).
- 359 4. Grim, J.Q. et al. Continuous-wave biexciton lasing at room temperature using solution-  
360 processed quantum wells. *Nature Nanotech.* **9**, 891-895 (2014).
- 361 5. Grivas, C. et al. Single-mode tunable laser emission in the single-exciton regime from  
362 colloidal nanocrystals. *Nature Commun.* **4**, 2376 (2013).
- 363 6. Dang, C. et al. Red, green and blue lasing enabled by single-exciton gain in colloidal  
364 quantum dot films. *Nature Nanotech.* **7**, 335-339 (2012).
- 365 7. Wang, Y. et al. Blue Liquid Lasers from Solution of CdZnS/ZnS Ternary Alloy Quantum  
366 Dots with Quasi-Continuous Pumping. *Adv. Mater.* **27**, 169-175 (2015).
- 367 8. Klimov, V.I., Mikhailovsky, A.A., McBranch, D.W., Leatherdale, C.A. & Bawendi, M.G.  
368 Quantization of multiparticle Auger rates in semiconductor quantum dots. *Science* **287**,  
369 1011-1013 (2000).
- 370 9. Lee, M.M., Teuscher, J., Miyasaka, T., Murakami, T.N. & Snaith, H.J. Efficient Hybrid  
371 Solar Cells Based on Meso-Superstructured Organometal Halide Perovskites. *Science*  
372 **338**, 643-647 (2012).
- 373 10. Zhou, H. et al. Interface engineering of highly efficient perovskite solar cells. *Science*  
374 **345**, 542-546 (2014).
- 375 11. Deschler, F. et al. High Photoluminescence Efficiency and Optically Pumped Lasing in  
376 Solution-Processed Mixed Halide Perovskite Semiconductors. *J. Phys. Chem. Lett.* **5**,  
377 1421-1426 (2014).
- 378 12. Zhu, H. et al. Lead halide perovskite nanowire lasers with low lasing thresholds and high  
379 quality factors. *Nature Mater.* **14**, 636-642 (2015).
- 380 13. Wang, Y. et al. All-Inorganic Colloidal Perovskite Quantum Dots: A New Class of  
381 Lasing Materials with Favorable Characteristics. *Adv. Mater.* **27**, 7101-7108 (2015).
- 382 14. Yakunin, S. et al. Low-threshold amplified spontaneous emission and lasing from  
383 colloidal nanocrystals of caesium lead halide perovskites. *Nature Commun.* **6** (2015).
- 384 15. Li, X. et al. CsPbX<sub>3</sub> Quantum Dots for Lighting and Displays: Room-Temperature  
385 Synthesis, Photoluminescence Superiorities, Underlying Origins and White Light-  
386 Emitting Diodes. *Adv. Funct. Mater.* **26**, 2435-2445 (2016).
- 387 16. Song, J. et al. Quantum Dot Light-Emitting Diodes Based on Inorganic Perovskite  
388 Cesium Lead Halides (CsPbX<sub>3</sub>). *Adv. Mater.* **27**, 7162-7167 (2015).
- 389 17. Protesescu, L. et al. Nanocrystals of Cesium Lead Halide Perovskites (CsPbX<sub>3</sub>, X = Cl,  
390 Br, and I): Novel Optoelectronic Materials Showing Bright Emission with Wide Color  
391 Gamut. *Nano Lett.* (2015).
- 392 18. Akkerman, Q.A. et al. Tuning the Optical Properties of Cesium Lead Halide Perovskite  
393 Nanocrystals by Anion Exchange Reactions. *J. Am. Chem. Soc.* **137**, 10276-10281 (2015).
- 394 19. Nedelcu, G. et al. Fast Anion-Exchange in Highly Luminescent Nanocrystals of Cesium  
395 Lead Halide Perovskites (CsPbX<sub>3</sub>, X = Cl, Br, I). *Nano Lett.* **15**, 5635-5640 (2015).
- 396 20. Swarnkar, A. et al. Colloidal CsPbBr<sub>3</sub> Perovskite Nanocrystals: Luminescence beyond  
397 Traditional Quantum Dots. *Angew. Chem., n/a-n/a* (2015).
- 398 21. Eaton, S.W. et al. Lasing in robust cesium lead halide perovskite nanowires. *Proc. Nat.*  
399 *Acad. Sci. U.S.A.* **113**, 1993-1998 (2016).
- 400 22. Eaton, S.W., Fu, A., Wong, A.B., Ning, C.-Z. & Yang, P. Semiconductor nanowire lasers.  
401 *Nature Reviews Materials* **1**, 16028 (2016).

- 402 23. Feng, L., Wong, Z.J., Ma, R.-M., Wang, Y. & Zhang, X. Single-mode laser by parity-  
403 time symmetry breaking. *Science* **346**, 972-975 (2014).
- 404 24. Xiao, Y. et al. Single-Nanowire Single-Mode Laser. *Nano Lett.* **11**, 1122-1126 (2011).
- 405 25. Sale, T.E. & Sale, T.E. Vertical cavity surface emitting lasers. (Research Studies Press,  
406 1995).
- 407 26. Yoshikawa, T. et al. Complete polarization control of 8×8 vertical-cavity surface-  
408 emitting laser matrix arrays. *Appl. Phys. Lett.* **66**, 908-910 (1995).
- 409 27. Chen, R., Sun, H.D., Wang, T., Hui, K.N. & Choi, H.W. Optically pumped ultraviolet  
410 lasing from nitride nanopillars at room temperature. *Appl. Phys. Lett.* **96**, 241101 (2010).
- 411 28. Sun, H.D. et al. Low-loss 1.3- $\mu\text{m}$  GaInNAs saturable Bragg reflector for high-power  
412 picosecond neodymium lasers. *Opt. Lett.* **27**, 2124-2126 (2002).
- 413 29. Calvez, S. et al. 1.3  $\mu\text{m}$  GaInNAs optically-pumped vertical cavity semiconductor  
414 optical amplifier. *Electron. Lett* **39**, 100-102 (2003).
- 415 30. Chen, S. et al. Gain-switching dynamics in optically pumped single-mode InGaN  
416 vertical-cavity surface-emitting lasers. *Opt. Express* **22**, 4196-4201 (2014).
- 417 31. Marra, D.C., Aydil, E.S., Joo, S.-J., Yoon, E. & Srdanov, V.I. Angle-dependent  
418 photoluminescence spectra of hydrogenated amorphous silicon thin films. *Appl. Phys.*  
419 *Lett.* **77**, 3346-3348 (2000).
- 420 32. Qiao, H. et al. Optical properties of II-VI colloidal quantum dot doped porous silicon  
421 microcavities. *Appl. Phys. Lett.* **96**, 161106 (2010).
- 422 33. Wang, Y. et al. Nonlinear Absorption and Low-Threshold Multiphoton Pumped  
423 Stimulated Emission from All-Inorganic Perovskite Nanocrystals. *Nano Lett.* **16**, 448-453  
424 (2016).
- 425 34. Samuel, I.D.W., Nanddas, E.B. & Turnbull, G.A. How to recognize lasing. *Nature Photon.*  
426 **3**, 546-549 (2009).
- 427 35. Chen, Q., Kiraz, A. & Fan, X. Optofluidic FRET lasers using aqueous quantum dots as  
428 donors. *Lab on a Chip* **16**, 353-359 (2016).
- 429 36. Adachi, M.M. et al. Microsecond-sustained lasing from colloidal quantum dot solids.  
430 *Nature Commun.* **6** (2015).
- 431 37. Makarov, N.S. et al. Spectral and Dynamical Properties of Single Excitons, Biexcitons,  
432 and Trions in Cesium–Lead-Halide Perovskite Quantum Dots. *Nano Lett.* **16**, 2349-2362  
433 (2016).
- 434 38. Liao, Q. et al. An Organic Microlaser Array Based on a Lateral Microcavity of a Single  
435 J-aggregation Microbelt. *Angew. Chem. Int. Ed.* **54**, 7037-7041 (2015).
- 436 39. Mhibik, O. et al. An ultra-narrow linewidth solution-processed organic laser. *Light Sci*  
437 *Appl* **5**, e16026 (2016).
- 438 40. Xu, D. et al. Polariton lasing in a ZnO microwire above 450 K. *Appl. Phys. Lett.* **104**,  
439 082101 (2014).
- 440 41. Oron, D., Kazes, M. & Banin, U. Multiexcitons in type-II colloidal semiconductor  
441 quantum dots. *Phys. Rev. B* **75**, 035330 (2007).
- 442 42. Xu, Y. et al. Two-Photon-Pumped Perovskite Semiconductor Nanocrystal Lasers. *J. Am.*  
443 *Chem. Soc.* **138**, 3761-3768 (2016).
- 444 43. Kemp, A.J. et al. Thermal management in vertical-external-cavity surface-emitting lasers:  
445 finite-element analysis of a heatspreader approach. *IEEE J. Quantum Electron.* **41**, 148-  
446 155 (2005).
- 447 44. Fan, F., Turkdogan, S., Liu, Z., Shelhammer, D. & Ning, C.Z. A monolithic white laser.  
448 *Nature Nanotech.* **10**, 796-803 (2015).
- 449 45. Wang, Y. et al. Unraveling the ultralow threshold stimulated emission from CdZnS/ZnS  
450 quantum dot and enabling high-Q microlasers. *Laser Photonics Rev.* **9**, 507-516 (2015).

452 **Acknowledgements**

453 This research is supported by the Singapore National Research Foundation through the  
454 Competitive Research Programme (CRP) under Project No. NRFCRP6-2010-02, the Singapore  
455 Ministry of Education through the Academic Research Fund under Projects Tier 1- RG92/15 and  
456 MOE 2011-T3-1-005 (Tier 3), and National Basic Research Program of China (grant number  
457 2014CB931700).

458 **Author contribution**

459 All authors contributed extensively to this work. Y.W. and V.N. conducted spectroscopic  
460 experiment and analysis. Y.W. and H.S. conceived and fabricated the VCSEL structure. X.L. and  
461 H.Z. synthesized the IPNC samples. H.S. and H.Z. supervised the project. Y.W., X.L., V.N., H.Z.,  
462 and H.S. analyzed data and interpreted the results, and wrote the manuscript with input from all  
463 authors.

464